Engineering Structures 44 (2012) 304–311

Contents lists available at SciVerse ScienceDirect

Engineering Structures

journal homepage: www.elsevier.com/locate/engstruct

Effect of local buckling core plate restraint in buckling restrained braces

T. Takeuchi [a,*], J.F. Hajjar [b,2], R. Matsui [a,1], K. Nishimoto [c,3], I.D. Aiken [d,4]

[a] Department of Architecture and Building Engineering, Tokyo Institute of Technology, M1-29, 2-12-1 Ookayama, Meguro-ku, Tokyo 152-8550, Japan
[b] Department of Civil and Environmental Engineering, Northeastern University, 400 Snell Engineering Center, 360 Huntington Avenue, Boston, MA 02115, USA
[c] Building Construction & Steel Structure Division, Nippon Steel Engineering Co. Ltd., Osaki Center Building, 1-5-1 Osaki, Shinagawa-ku, Tokyo 141-8604, Japan
[d] Seismic Isolation Engineering, Inc., 1144 65th St., Unit D Emeryville 94608-1053, CA, USA

ARTICLE INFO

Article history:
Received 9 August 2011
Revised 15 May 2012
Accepted 17 May 2012
Available online 13 July 2012

Keywords:
Steel structures
Seismic
Buckling restrained brace
Local buckling failure

ABSTRACT

Buckling-Restrained Braces (BRBs) are commonly used as ductile bracing elements in seismic zones. Key limit states governing BRB design include preventing both flexural buckling and local buckling failures. In this study, the authors propose a strategy for the prevention of in-plane local buckling failure of a BRB whose restrainer is composed of a mortar in-filled circular or rectangular steel tube with various mortar thicknesses. Cyclic loading tests on BRBs possessing various mortar restrainers and circular tube thicknesses were carried out to investigate the effect of the mortar and the sectional shape of the restraint tube on the local buckling failure of buckling-restrained braces.

1. Introduction

Buckling-Restrained Braces (BRB) and their frames (BRBF) have been extensively used for seismic applications over the last twenty years in seismic zones as Japan, US, Taiwan, and China, etc.; however, their design criteria is not necessarily established yet. In the AIJ recommendation for Stability Design [1], the design criteria for BRBs are indicated as follows; (1) Restrainer design to prevent overall buckling, (2) Effective clearance between core and restrainer to achieve stable hysteresis, (3) Core plate local buckling failure prevention, (4) Connection design to guarantee core yield, (5) Overall stability design including connections, and (6) Cumulative deformation capacity until core fracture. However, much of the past work on BRBs focused on the response characteristics and seismic performances of BRBFs, while little work on the design criteria for the BRB itself has been reported [2–7].

For criterion (3) above related to the restrainer conditions to prevent local buckling failure of the core plates, Koetaka et al. [2] have indicated that the out-of-plane local buckling wave length are governed by the thickness and plastic modulus of the core plates, and Chou et al. [6] discussed the criteria of the restrainer conditions to prevent out-of-plane local buckling. However, ordinary BRBs with a mortar in-filled steel tube restrainer have risks of local buckling failure in the in-plane direction as seen in Fig. 1, and research on this criterion is very limited. Recently, while investigating optimal economic configurations for BRBs, restrainers with smaller thickness tubes were employed along with thick core plates, thus increasing the risks of in-plane local buckling failure.

The authors have proposed an evaluation strategy for the prevention of in-plane local buckling failure of rectangular BRBs [5] based on experimental tests and numerical simulations; however, this work focused on rectangular tubes where the effect of the mortar thickness at the edge of the core plate was small. For designing economical BRBs, not only rectangular but circular restraint tubes with various mortar thicknesses may be employed, and the proposed criteria in the prior study [5] are incomplete for these configurations.

In this study, cyclic loading tests on BRB specimens are carried out to confirm the effect of the mortar thickness and the restraint tube sections for in-plane local buckling failure of BRBs. Based on these results, the criteria necessary to prevent such local buckling failure is reconstituted including the effects outlined above.

2. Uniaxial cyclic loading tests on BRBs for various mortar and circular restraint tube thickness

The experimental test setup and associated specimens are shown in Table 1 and Fig. 2. Hereafter, specimen labels are defined as RY65M25; the first character represents the shape of the restrainer; R is a rectangular shape; C is a circular shape. The second

* Corresponding author. Tel./fax: +81 3 5734 3165.
E-mail addresses: ttoru@arch.titech.ac.jp (T. Takeuchi), jf.hajjar@neu.edu (J.F. Hajjar), matsui.r.aa@m.titech.ac.jp (R. Matsui), nishimoto.kohji1@eng.nsc.co.jp (K. Nishimoto), ida@siecorp.com (I.D. Aiken).
[1] Tel./fax: +81 3 5734 3165.
[2] Tel.: +1 617 373 3242; fax: +1 617 373 4419.
[3] Tel.: +81 3 3275 5114; fax: +81 3 3275 5978.
[4] Tel.: +1 510 774 5818; fax: +1 510 595 7499.

0141-0296/$ - see front matter © 2012 Elsevier Ltd. All rights reserved.
http://dx.doi.org/10.1016/j.engstruct.2012.05.026

Nomenclature

A_c	cross-section area of core plate plastic zone
A_e	cross-section area of core plate elastic zone
B_c	width of core plate
B_r	width of restrainer wall
c_m	contribution factor of mortar
E	elastic modulus of core plate
$E_{tc.}$	tangent modulus of core plate
L_e	elastic zone length in the range of initial gage length
L_g	initial gage length
L_p	length of plastic zone of core plate
l_p	length of local buckling wave of core plate
M_p	plastic hinge moment of restrainer wall
P_c	core plate axial force
P_{cy}	yield axial force of core plate
P_{lb}	local buckling failure force of core plate
P_r	perpendicular force of core plate
P_{rlb}	ultimate perpendicular force of core plate
P_{ry}	plane yielding force of restraint tube
s	clearance between core plate and restrainer
t_c	thickness of core plate
t_m	thickness of mortar
t_r	thickness of restraint tube
α	hardening ratio of strength after yielding
δ_c	displacement of core plate
δ_g	extensometer displacement
ε_c	strain of plastic zone of core plate
ε_t	maximum tensile strain of core plate
ε_r	strain of restrainer wall
γ	local buckling failure index
ν_p	plastic Poisson's ratio
θ	angle between application point of perpendicular force component and strong centroid axis of core plate
σ_{cy}	yield stress of core plate
σ_{ry}	yield stress of restrainer wall

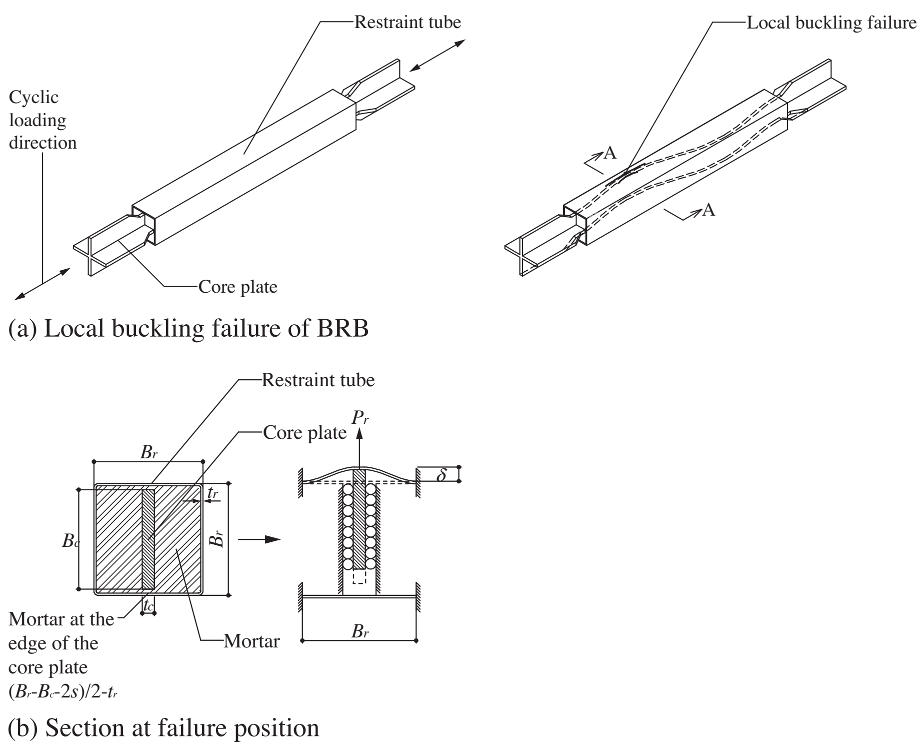

Fig. 1. Local buckling failure of core plate in BRB.

Table 1
Specimen parameters.

Specimen	L_g (mm)	L_p (mm)	B_r (mm)	t_r (mm)	σ_{ry} (N/mm^2)	B_c (mm)	t_c (mm)	$\boldsymbol{\sigma_{cy}}$ (N/mm)	$E_{tc.}$ (N/mm^2)	Mortar thickness at the edge of core plate (mm)	l_p (mm)	s (mm)	ε_t	a	P_r (kN)	P_{rlb} (kN)	y (Ref. [5])
RY65M7*				2.3	350	130	16	261	4100	6.7	467.3	1.0	0.03	1.4	6.4	3.7	0.6
RY65M25			150							24.7					6.9	2.9	0.4
RY76M37	1550	1000	175		273	94	22	245		37.2						3.4	0.5
CY83M15*				2.0	231			261		14.6					6.4	2.0	0.3
CY110M15			165.2	1.5	280	130	16	257		15.1					6.3	1.3	0.2
CY138M15				1.2	136					15.4						0.4	0.06

* Experimental results shown here are reported in prior work.

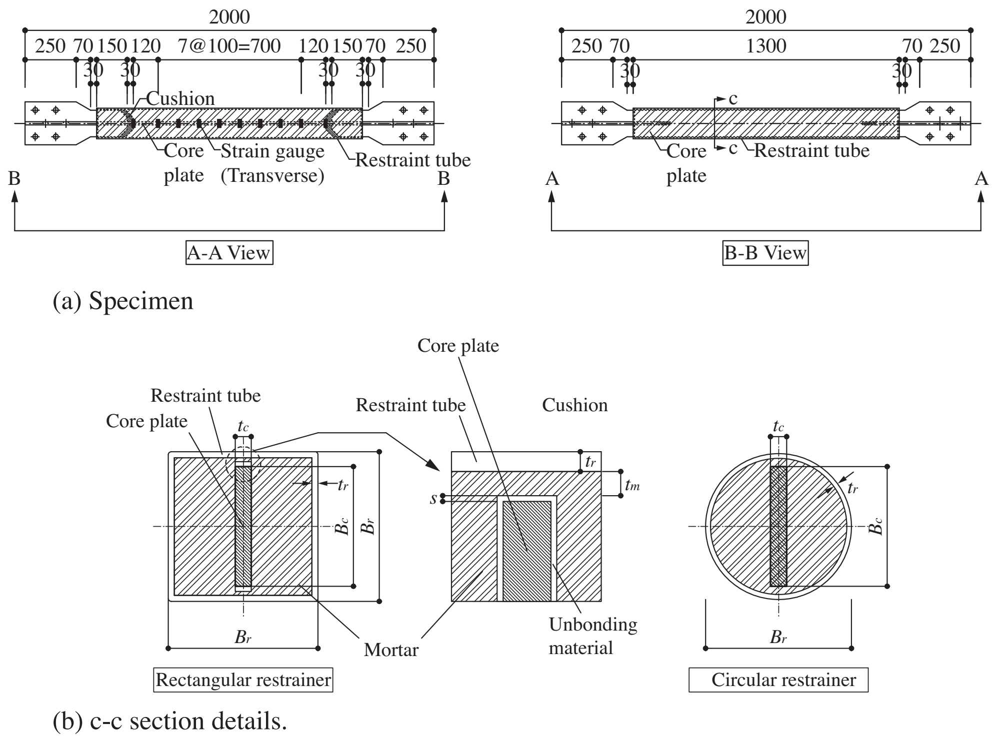

Fig. 2. Specimens for uniaxial cyclic loading tests.

Table 2
Rectangular restraint tube BRB cyclic loading test results and revised failure index.

Specimen	Cycle	ε_t	α	B_r (mm)	t_r (mm)	σ_{ry} (N/mm)	B_c (mm)	t_c (mm)	σ_{cy} (N/mm)	$E_{tc.}$ (N/mm)	Mortar thickness at the edge of core plate t_m (mm)	l_p (mm)	s (mm)	P_r (kN)	P_{rlb} (kN)	γ (Revised)	Local Buckling Failure
	0.50%	0.006	1.14	150	2.3	273	94	22	245	4100	24.7	348.8	1.0	3.8	6.5	1.74	None
RY65M25	1.00%	0.011	1.36											4.9		1.33	
	2.00%	0.021	1.5											7.0		0.93	
	3.00%	0.031	1.75											8.7		0.75	Occur
RY76M37	0.50%	0.006	1.13	175	2.3	273	94	22	245	4100	37.2	348.8	1.0	3.7	8.4	2.27	None
	1.00%	0.011	1.34											4.9		1.73	
	2.00%	0.021	1.5											7.0		1.20	
	3.00%	0.030	1.8											9.0		0.93	Occur
	0.50%	0.005	1.14	150	2.3	273	130	16	245	4100	6.7	482.4	1.0	2.8	3.7	1.31	None
RY65M7 (Ref.[5])	1.00%	0.010	1.36											3.8		0.97	
	2.00%	0.020	1.4											5.7		0.65	Occur
	3.00%	0.032	1.8											8.1		0.46	

Table 3
Circular restraint tube BRB cyclic loading test results and revised failure index.

Specimen	Cycle	ε_t	α	B_r (mm)	t_r (mm)	σ_{ry} (N/mm)	B_c (mm)	t_c (mm)	σ_{cy} (N/mm)	$E_{tc.}$ (N/mm)	Mortar thickness at the edge of core plate t_m (mm)	l_p (mm)	s (mm)	P_r (kN)	P_{rlb} (kN)	γ (Revised)	Local buckling failure
CY110M15	0.50%	0.006	1.08	165.2	1.5	280	130	16	257	4100	15.1	470.9	1.0	2.9	72.4	25.0	None
	1.00%	0.011	1.27											3.9		18.7	
	2.00%	0.021	1.53											5.8		12.5	
	3.00%	0.031	1.80											8.1		8.9	
CY138M15	0.50%	0.006	1.08	165.2	1.2	280	130	16	257	4100	15.4	470.9	1.0	2.9	58.5	20.2	None
	1.00%	0.011	1.28											3.9		15.0	
	2.00%	0.020	1.54											5.8		10.1	
	3.00%	0.031	1.8											8.2		7.2	
	0.50%	0.005	1.09	165.2	2.0	280	130	16	257	4100	14.6	470.9	1.0	2.9	94.7	32.5	None
CY83M16	1.00%	0.010	1.31											4.0		23.7	
(Ref. [5])	2.00%	0.020	1.57											5.9		15.9	
	3.00%	0.030	1.8											8.3		11.4	

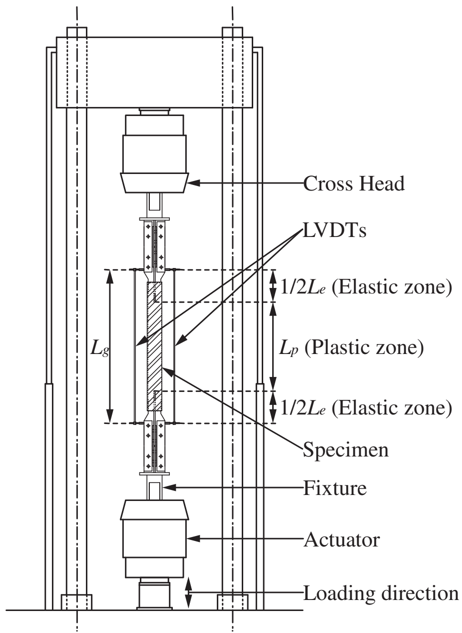

Fig. 3. Specimen and setup for uniaxial cyclic loading tests.

character denotes the loading pattern; Y represents cyclic loading. The third number indicates the width-to-thickness or diameter-to-thickness ratio of the restrainer steel tube. M25 represents the mortar thickness t_m between the edge of the core plate and the restrainer as seen in Fig. 2b, which is a newly introduced parameter in this paper. Unbonding material is used to create a gap between the core and the mortar; however, the stiffness and strength of this material are very small and are considered to be negligible for restraining the core plates (see Tables 2 and 3).

The index γ in Table 1 is the safety factor proposed by the authors [5], where the effect of the mortar was neglected. For instance, the index γ for RY65M25 was 0.4, which indicates the strength of RY65M25 was weaker than that of RY65M7, whose γ was 0.6. The width-to-thickness ratios of the rectangular restrainer varied between 65 and 76, and the diameter-to-thickness ratio of the circular restrainer ranged from 110 to 138. Strain gauges were attached on the surface of the restrainer along its length, oriented transversely to measure bulging due to local buckling, as shown in Fig. 2a (A–A view); s is the clearance between the core plate and the restrainer. To investigate the effect of mortar thickness, the size of the core plates were 16 mm × 130 mm and 22 mm × 94 mm (these have the same cross-sectional areas), comparable to the monotonic compression tests in [5], and cyclic loading was applied as in Fig. 3. The axial force was measured by a load cell in the testing machine, and the axial displacement of the BRB is measured by extensometers between both end plates over length L_g as shown in Table 1 and Fig. 3. The displacement of the plastic zone of the core plate is defined as δ_c and is estimated by Eq. (1):

$$\delta_c = \delta_g - \frac{P_c}{A_e E} L_e \tag{1}$$

where δ_g is the extensometer displacement; P_c is the core plate axial force; A_e is the initial cross-section area of the core plate elastic zone; E (=205,000 N/mm^2) is the elastic modulus of the core plate; and L_e is the elastic zone length in the range of initial gage length. From this equation, the strain of the plastic zone of the core plate ε_c may be calculated by Eq. (2):

$$\varepsilon_c = \frac{\delta_c}{L_p} \tag{2}$$

where L_p is the length of the plastic zone of the core plate. The core plate stress σ_c is calculated by Eq. (3):

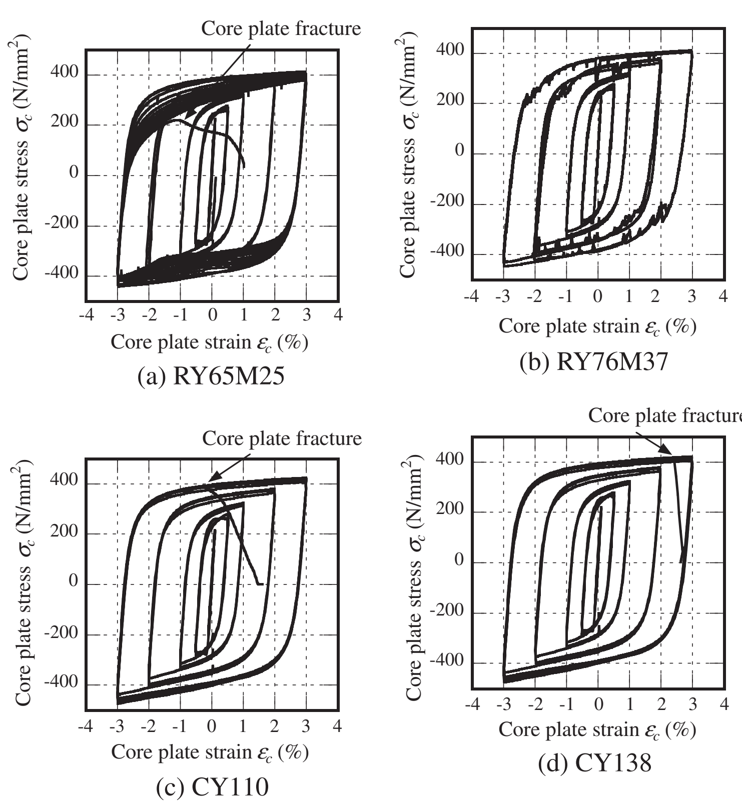

Fig. 4. Stress–strain curves for uniaxial cyclic loading tests.

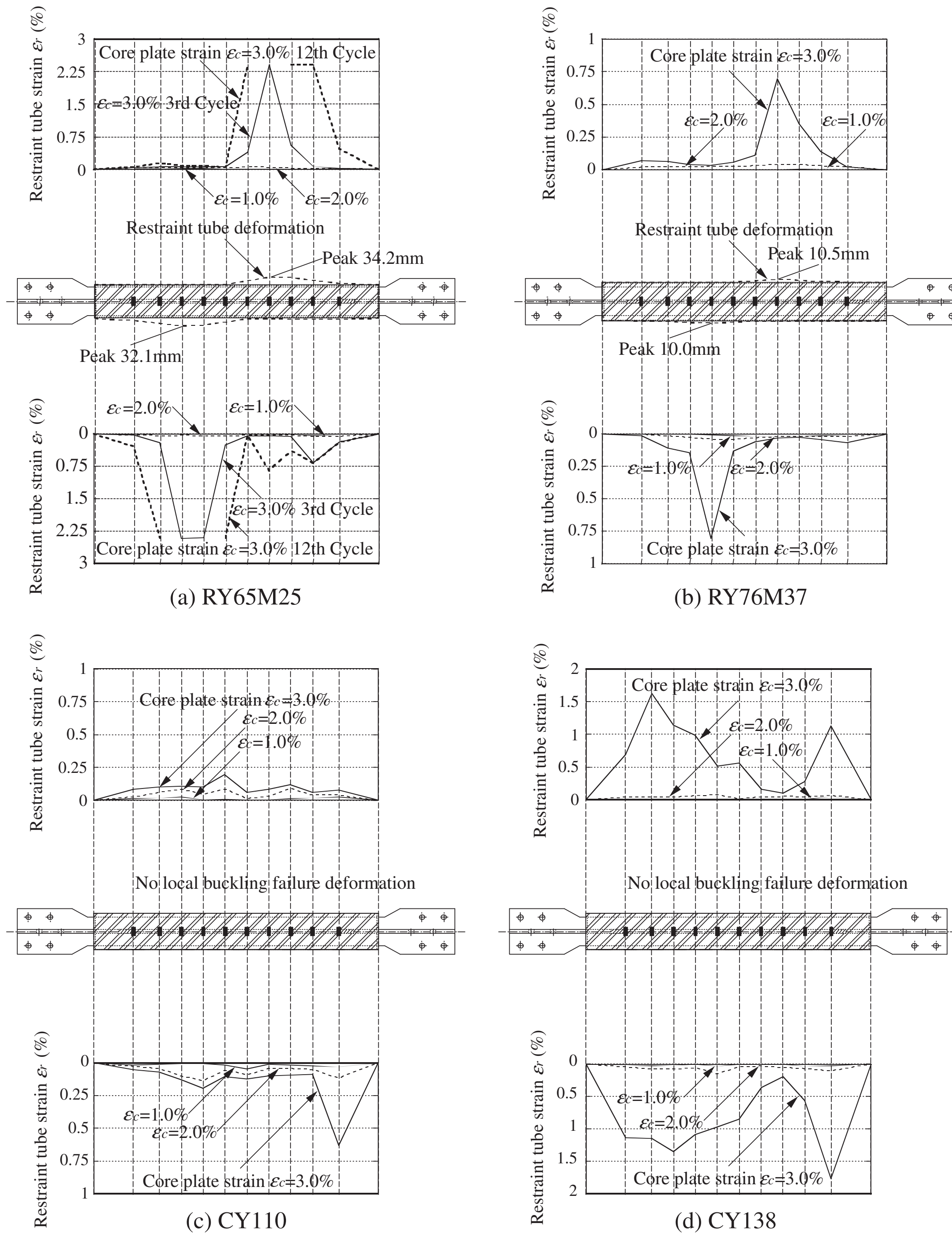

Fig. 5. Restraint tube strain and deformation.

$$\sigma_c = \frac{P_c}{A_c} \tag{3}$$

where A_c is the cross-section area of the core plate plastic zone. The cyclic loading was applied with amplitudes of $\varepsilon_c = \pm 0.5\%$, $\pm 1.0\%$, $\pm 2.0\%$, and $\pm 3.0\%$, with three cycles each. The hysteresis curves of the core plate as obtained from the tests are shown in Fig. 4, and strain transitions at the surface of the restrainer wall as measured by the strain gauges are shown in Fig. 5. Specimens RY65M25 and RY65M37, having thicker mortar between the edge of the core plate and the restrainer, exhibited a local buckling failure at 3% strain amplitude of the core plate (Fig. 5a, b, and Fig. 6). RY65M7 exhibited local buckling failure at 2% strain amplitude of the core plate in the previous study [5], thus the occurrence of the local buckling failure of RY65M25 and RY76M37 is later than RY65M7. Therefore, the mortar thickness between the edge of the core plate and the restrainer prevents the local buckling failure. The circular restraint tube strain in Fig. 5c and d increased to approximately 0.8% when 3% strain amplitude of the core plate was achieved. However, specimens CY110M15 and CY138M15, with a thinner circular restrainer wall than specimen CY83M16 in the previous study [5], showed no local buckling failure even with high D/t ratio and displayed stable stress–strain curves until the low-cycle fatigue fracture of their core plates, which was similar to specimen CY83M16.

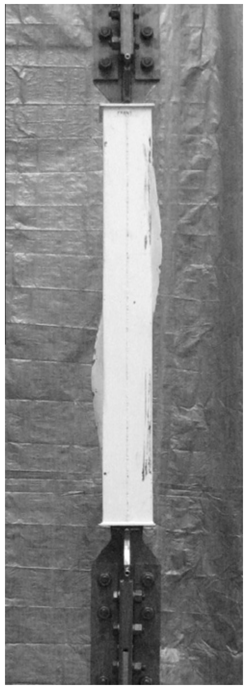

Fig. 6. Local buckling failure of RY65M25 (after testing).

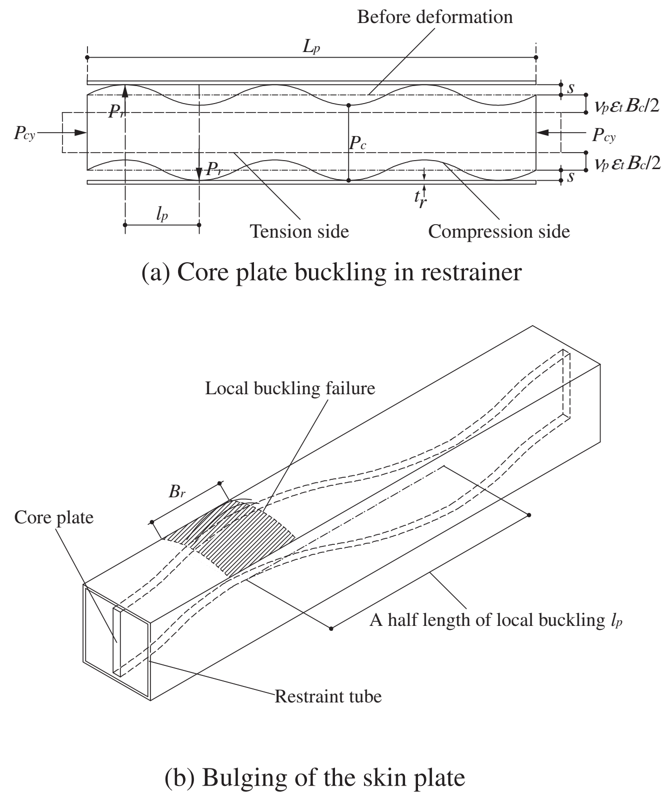

Fig. 7. Collapse model of restrainer wall at local buckling failure.

3. Re-evaluation of local buckling failure criteria for rectangular restraint tube

From the previous work, the perpendicular force of the core plate may be calculated as Eq. (4), as shown in Fig. 7a.

$$P_r = \frac{2s + v_p\varepsilon_t B_c}{l_p} P_{cy} = \frac{2s + v_p\varepsilon_t B_c}{l_p} B_c t_c \alpha\sigma_{cy} \tag{4}$$

where s is the clearance between the core and the restrainer, v_p is the plastic Poisson's ratio $v_p = 0.5$, ε_t is the maximum tensile strain of the core plate, P_{cy} is the yield axial force of the core plate, σ_{cy} is the yield stress of the core plate, t_c is the thickness of the core plate, α is the ratio representing the increase in material strength after yielding (α = 1.1–1.8), and l_p is the length of the local buckling wave of the core plate estimated by Eq. (5), which generally is approximately 4 times the core plate width B_c. This evaluation is similar to out-of-plane local buckling indicated in prior studies [2,6].

$$l_p = \frac{\pi B_c}{2}\sqrt{\frac{E_{tc}}{3\sigma_{cy}}} \tag{5}$$

where $E_{tc.}$ is the tangent modulus of the core plate. The shaded area in Fig. 7b shows the bulging of the restrainer tube skin plate, which indicates a collapse of the restrainer tube. After estimating the collapse mechanism considering the effect of mortar as shown in Fig. 8, the perpendicular force component can be calculated by Eqs. (6) and (7):

$$M_p = \frac{B_r t_r^2}{4}\sigma_{ry} \tag{6}$$

$$P_{rlb} = \frac{8M_p}{B_r - t_c - c_m t_m} = 2t_r^2\sigma_{ry}\frac{B_r}{B_r - t_c - c_m t_m} \tag{7}$$

In these equations, σ_{ry} is the yield stress of the restrainer wall, B_r is the width of the restrainer tube, t_m is the mortar thickness, t_r is the restrainer wall thickness, c_m is the contribution factor of the mortar. Here, c_m of the rectangular restrainer is configured as 2.5 from current experimental results. In Eq. (7), the proposed equation in earlier work [5] is obtained by neglecting the effect of t_m and t_c. The ratio γ is then defined by Eq. (8) as the ultimate strength of the restrainer wall P_{rlb} divided by the perpendicular force component of the core plate P_r:

$$\gamma = \frac{P_{rlb}}{P_r} = \frac{2t_r^2}{B_c t_c}\frac{l_p}{2s + v_p\varepsilon_t B_c}\frac{\sigma_{ry}}{\alpha\sigma_{cy}}\frac{B_r}{B_r - t_c - c_m t_m} \tag{8}$$

The ratio γ represents the local buckling failure index; $\gamma > 1.0$ means that the restrainer is sufficient to prevent local buckling failure. The axial force P_{lb} causing the local buckling failure can be calculated by Eqs. (9) and (10) as follows:

$$P_{lb} = 2t_r^2\frac{l_p}{2s + v_p\varepsilon_t B_c}\sigma_{ry}\frac{B_r}{B_r - t_c - c_m t_m} \tag{9}$$

$$\gamma = \frac{P_{lb}}{\alpha P_{cy}} \tag{10}$$

The γ indices estimated from the test specimens of the rectangular restraint tube are shown in Fig. 10a together with the occurrence of local buckling failure. From this figure, it is observed that all specimens that caused local buckling failure had a γ value less than 1.0, and the criterion for the restrainer wall is substantiated well by this index.

4. Discussion of local buckling failure criteria for circular restraint tube

When the restraint tube is circular, the restraint tube is assumed to resist the perpendicular force from the core plate by in-plane stress. An estimated collapse mechanism with a circular restrainer is shown Fig. 9. From this estimation, the ultimate perpendicular force component P_{rlb} is calculated as shown in Eq. (11):

$$P_{rlb} = 2P_{ry}\cos\theta = \pi\sigma_{ry}t_r B_r\cos\theta \tag{11}$$

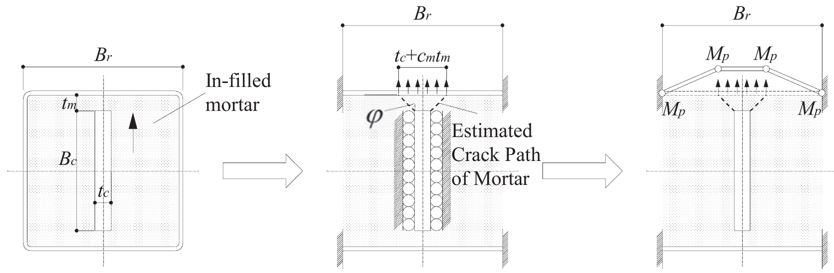

Fig. 8. Failure mechanism of rectangular restraint tube considering effect of mortar.

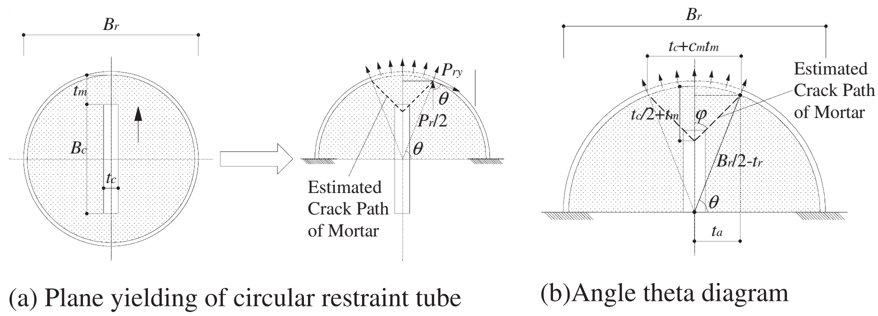

Fig. 9. Local buckling failure mechanism for circular restraint tube.

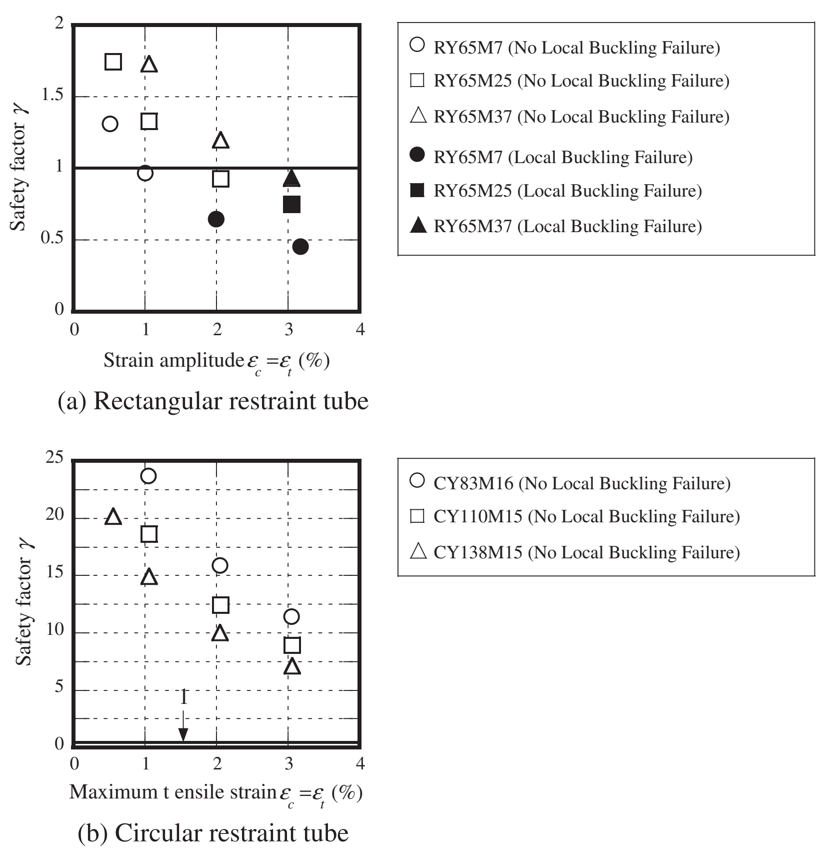

Fig. 10. Safety factor evaluation.

where P_{ry} is the in-plane yield strength of the restraint tube skin, and θ indicates the angle between the application point of the perpendicular force component and the strong centroid axis of the core plate as Fig. 9b. The cosine of the angle is calculated as Eq. (12).

$$\cos\theta = \frac{c_m t_m + t_c}{B_r - 2t_r} \tag{12}$$

Here c_m of the circular restrainer is estimated as 2.5 from current experimental results, and is the same as for the rectangular restrainers. Similarly to Eqs.(8), (9), the failure index γ for the circular restraint tube is calculated to Eq. (13), and the local buckling failure force P_{lb} of the core plate for the circular restraint tube is estimated as Eq. (14).

$$\gamma = \frac{P_{rlb}}{P_r} = \frac{\pi t_r}{B_c t_c} \frac{l_p}{2s + \nu_p \varepsilon_t B_c} \frac{\sigma_{ry}}{\alpha \sigma_{cy}} B_r \frac{c_m t_m + t_c}{B_r - 2t_r} \tag{13}$$

$$P_{lb} = \pi t_r \frac{l_p}{2s + \nu_p \varepsilon_t B_c} \sigma_{ry} B_r \frac{c_m t_m + t_c}{B_r - 2t_r} \tag{14}$$

where B_r is the diameter of the circular restrainer tube, and all other variables are the same as those for the rectangular restraint tube. Fig. 10b shows the indices estimated from test specimens of the circular restraint tube. The index γ of the circular restraint tube represents a much higher value than 1.0, which explains the reason why no circular restraint tube showed a local buckling failure in spite of the high D/t ratios.

5. Conclusions

In this study, experiments were carried out using buckling-restrained braces composed of steel core plates and mortar-filled steel tube restrainers. The work focused on exploring the local buckling failure strength of buckling-restrained braces, focusing on the effect of the mortar thickness and the sectional shape of the restrainer. As a result, the following conclusions were obtained:

(1) Local buckling failures were observed in specimens possessing rectangular tubes with a width-to-thickness ratio of 65 and 76. The initiation of local buckling failure started later as the mortar thickness increased, and the effect of the mortar thickness was observed.
(2) The criteria for the local buckling failure of BRBs can be modified by the mortar thickness and the restraint tube shape. The revised criteria improve the ability to predict local buckling failure in BRBs.
(3) With a circular restraint tube, local buckling failure did not occur until the core plate plastic strain amplitude was 3%, even for large diameter-to-thickness ratios of the tube.

Acknowledgements

This research was supported by Nippon Steel Engineering Co., Ltd. and the University of Illinois at Urbana-Champaign. The authors thank Joshua Steelman, Grzegorz Banas, and Timothy Prunkard of the University of Illinois at Urbana-Champaign, and Yu Nakamura at the Tokyo Institute of Technology for their contributions to the experiments conducted in this research. Any opinions, findings, and conclusions or recommendations expressed in this material are those of the authors and do not necessarily reflect the views of the sponsors.

References

[1] Architectural Institute of Japan. Recommendations for stability design of steel structures. Sec. 3.5 buckling restrained brace; 2009. p. 74–9 [in Japanese].
[2] Koetaka Y, Byakuno Y, Inoue I. Experimental verification of design criteria of knee brace damper. 8th Taiwan-Korea-Japan joint seminar on earthquake engineering for building structures; 2006. p. 69–79.
[3] Chou CC, Chen PJ. Compressive behavior of central gusset plate connections for a buckling-restrained braced frame. J Construct Steel Res 2009;65:1138–48.
[4] Wigle VR, Fahnestock LA. Buckling-restrained frame connection performance. J Construct Steel Res 2010;66:65–74.
[5] Takeuchi T, Hajjar J, Matsui R, Nishimoto K, Aiken I. Local buckling restraint condition for core plates in buckling restrained braces. J Construct Steel Res 2010;66:139–49.
[6] Chou CC, Chen SY. Subassemblage tests and finite element analyses of sandwiched buckling–restrained braces. Eng Struct 2010;32:2108–21.
[7] Hikino T, Okazaki T, Kajiwara K, Nakashima M. Out-of-plane stability of buckling restrained braces for advanced seismic performance. In: Proceedings of structural congress, ASCE; 2011.